WILEY JCN RESEARCH IN SYSTEMS NEUROLOGY
THE JOURNAL OF COMPARATIVE NEUROLOGY

RESEARCH ARTICLE

Neuronal response properties across cytochrome oxidase stripes in primate V2

Rafael Peres | Juliana G. M. Soares | Bruss Lima ⬤ | Mario Fiorani | Marco Chiorri | Maria M. Florentino | Ricardo Gattass ⬤

Programa de Neurobiologia, Instituto de Biofísica Carlos Chagas Filho, Universidade Federal do Rio de Janeiro, Rio de Janeiro, RJ, 21941-902, Brazil

Correspondence
Ricardo Gattass, Instituto de Biofísica Carlos Chagas Filho, Bloco G, CCS, Universidade Federal do Rio de Janeiro, Cidade Universitária, Ilha do Fundão, Rio de Janeiro, RJ 21941-902, Brazil.
Email: rgattass@gmail.com.

Abstract

Cytochrome oxidase histochemistry reveals large-scale cortical modules in area V2 of primates known as thick, thin, and interstripes. Anatomical, electrophysiological, and tracing studies suggest that V2 cytochrome oxidase stripes participate in functionally distinct streams of visual information processing. However, there is controversy whether the different V2 compartments indeed correlate with specialized neuronal response properties. We used multiple-electrode arrays (16 × 2, 8 × 4 and 4 × 4 matrices) to simultaneously record the spiking activity (N = 190 single units) across distinct V2 stripes in anesthetized and paralyzed capuchin monkeys (N = 3 animals, 6 hemispheres). Visual stimulation consisted of moving bars and full-field gratings with different contrasts, orientations, directions of motion, spatial frequencies, velocities, and color contrasts. Interstripe neurons exhibited the strongest orientation and direction selectivities compared to the thick and thin stripes, with relatively stronger coding for orientation. Additionally, they responded best to higher spatial frequencies and to lower stimulus velocities. Thin stripes showed the highest proportion (80%) of neurons selective to color contrast (compared to 47% and 21% for thick and interstripes, respectively). The great majority of the color selective cells (86%) were also orientation selective. Additionally, thin stripe neurons continued to increase their firing rate for stimulus contrasts above 50%, while thick and interstripe neurons already exhibited some degree of response saturation at this point. Thick stripes best coded for lower spatial frequencies and higher stimulus velocities. In conclusion, V2 CytOx stripes exhibit a mixed degree of segregation and integration of information processing, shedding light into the early mechanisms of vision.

KEYWORDS

cytochrome oxidase, MAP multichannel acquisition (RRID:SCR_003170), Plexon offline sorter (RRID:SCR_000012), primate electrophysiology, V2 stripes

1 | INTRODUCTION

Cortical columns are considered the basic building blocks of cortical organization (Hubel & Wiesel, 1968; Mountcastle, 1997). Within these structures, nearby neurons encode similar stimulus features, such as selectivity for position, orientation, direction, or color contrast. In addition to columns, the neocortex also exhibits modular organization on larger scales. For example, the second visual area (V2) of primates shows compartmental organization based on stripes that run orthogonal to the V1/V2 border. These V2 compartments can be revealed using histochemical staining for the mitochondrial enzyme cytochrome c oxidase (CytOx) and are comprised of CytOx-rich (thin and thick stripes) and CytOx-poor (interstripes) regions (DeYoe & Van Essen, 1985; Gattass et al., 1990; Livingstone & Hubel, 1983; Wong-Riley & Carroll, 1984; Zeki & Shipp, 1989).

Pioneering work by Livingstone and Hubel (1983,1984,1988) shed light into the functional organization of parallel visual pathways comprising early primate vision. These and other related studies offered an integrated view of how the modular architecture of areas V1 and V2 are associated with parallel pathways originating in the retina and relayed through the lateral geniculate nucleus (Carroll & Wong-Riley, 1984; DeYoe & Van Essen, 1985; Federer et al., 2009;

Gattass et al., 1990; Gattass, Sousa, Mishkin, & Ungerleider, 1997; Levitt, Kiper, & Movshon, 1994; Nakamura, Gattass, Desimone, & Ungerleider, 1993; Sousa, Piñón, Gattass, & Rosa, 1991; Zeki & Shipp, 1989). The proposed existence of a dorsal and a ventral stream of visual information processing advances the notion that parallel visual pathways extend all the way to higher associative areas (Ungerleider & Mishkin, 1982). Previously, we used CytOx histochemistry and retrograde tracer injections to study V2 connectivity in primates (Nascimento-Silva, Gattass, Fiorani, Jr., & Sousa, 2003; Nascimento-Silva, Pinõn, Soares, & Gattass, 2014). We found PO-projecting (i.e., parieto-occipital-projecting) neurons in thick and interstripes, MT-projecting (i.e., middle temporal-projecting) neurons almost exclusively in thick stripes, and V4-projecting neurons located mostly in thin and interstripes. Importantly, no double-labeled neurons were found suggesting limited superimposition of the pathways. These results favor the existence of three distinct streams diverging from V2 stripes: ventral (toward V4), dorsolateral (toward MT), and dorsomedial (toward PO).

Electrophysiological studies have corroborated the anatomical data in supporting a functional segregation of V2 pathways. The early work by Livingstone and Hubel (1983,1984,1988) showed that neurons located in thick stripes receive significant input from the magnocellular pathway and are relevant to the processing of visual information related to movement. On the other hand, thin and interstripes receive strong input from the parvocellular pathway. Interstripes code preferentially for stimulus orientation, which is relevant to form processing, while thin stripes are color-processing modules. Certain functional specializations attributed to specific V2 stripes, such as the strong orientation selectivity found in thick and interstripes (reviewed in Gegenfurtner, 2003) and the high prevalence of color-selective neurons in thin stripes (Gegenfurtner, Kiper, & Fenstemaker, 1996; Levitt et al., 1994; Peterhans & von der Heydt, 1993; Tamura, Sato, Katsuyama, Hata, & Tsumoto, 1996) have been corroborated by subsequent works (Kiper, Fenstemaker, & Gegenfurtner, 1997; Roe & Tso, 1995; Shipp & Zeki, 2002; Yoshioka & Dow, 1996). However, substantial discrepancies remain concerning the degree to which V2 stripes are functionally segregated (Federer et al., 2009; Federer, Williams, Ichida, Merlin, & Angelucci, 2013; Felleman et al., 2015; Levitt et al., 1994). For example, DeYoe & Van Essen (1985) found color-coding neurons not to be exclusive to thin stripes, and it might be incorrect to assume that color-coding neurons are generally nonselective for orientation (Livingstone & Hubel, 1984,1987).

Due to the potentially crucial role played by V2 modules in the integration of early and intermediate-level vision, we decided to investigate the premise that distinct functional properties, such as orientation and direction selectivity, and coding for contrast, spatial frequency, speed and color, are associated with specific V2 modules. As an advancement to previous approaches, we used multielectrode arrays (16 × 2, 8 × 4, and 4 × 4 matrices) capable of simultaneously sampling single-unit activity across the CytOx-defined thick, thin and interstripes of V2 in the anesthetized and paralyzed capuchin monkey.

2 | METHOD

2.1 | Animals

Area V2 of three adult *Sapajus apella* monkeys were studied in terminal experiments lasting 24–72 hours. The *Sapajus* (former genus *Cebus*) is a diurnal, medium-sized New-World primate, comparable to the Old-World monkey *Macaca fascicularis* in terms of brain size and sulcal pattern (Freese & Oppenheimer, 1981; Le Gros Clark, 1959). All experimental protocols were conducted following the National Institutes of Health (NIH) guidelines for animal research and were approved by the Committee for Animal Care and Use of the Health Science Center, Federal University of Rio de Janeiro (CEUA, IBCCF/ UFRJ 190-06/16).

2.2 | Surgical procedures

Before the recording session, a head bolt and a recording chamber were implanted on the skull of each monkey, under anesthesia and aseptic conditions. Using anatomical landmarks, we positioned the recording chamber so as to allow access to area V2. Before surgery, anesthesia was induced with 30 mg/kg (intramuscular or *im*) of ketamine hydrochloride (Ketalar™, Parke Davis, Rio de Janeiro, RJ, Brazil) and 8 mg/kg (*im*) of xylidine-tiazine chlorhydrate solution (Rompun™, Bayer; São Paulo, SP, Brazil). In addition, animals also received 0.15 mg/kg (*im*) of atropine sulfate (Atropina™, Roche; São Paulo, SP, Brazil) to reduce salivation and other secretions, and 0.8 mg/kg (*im*) of benzodiazepine (Valium™, Roche; São Paulo, SP, Brazil) to induce sedation. Animals were intubated with an endotracheal tube and anesthesia was maintained with 2% isoflurane (Fluothane™, AstraZeneca, São Paulo, SP, Brazil) in a 7:3 mixture of nitrous oxide and oxygen. Electrocardiogram, body temperature, and end-tidal CO_2 were monitored continuously to ensure anesthesia depth and animal well-being during surgery. Additionally, we continuously administered postsurgical analgesia at a rate of 0.85 µg/kg per hour for 3 days using a fentanyl skin patch (Durogesic; Janssen-Cilag, São Paulo, Brazil) and the antibiotic benzylpenicillin benzathine (Benzetacil – 300,000 U – Eurofarma). The animals were monitored for a few days after surgery to ensure their prompt recovery.

2.3 | Electroretinogram

In order to study color vision, we needed to ascertain which types of ones were present in each animal. We carried out electroretinograms (ERG) as described in Soares et al. (2010). Anesthesia was induced as described above (see **Surgical procedures**). The pupils were dilated with 1% tropicamide (Mydriacyl™, Alcon; São Paulo, SP, Brazil) and 10% phenylephrine hydrochloride (Fenilefrin™, Cristália; São Paulo. SP, Brazil). The ERG was obtained using a gold electrode attached to the contact lens. The signal was amplified, filtered (1–100 Hz, notch for 60 Hz), sampled, and recorded by PowerLab (ADInstruments; Sydney, Australia) using the LabChart 7.0 software. Visual stimuli were generated using Psychtoolbox (Brainard, 1997; Kleiner et al., 2007) run on MATLAB R2013b (The MathWorks, Inc., Natick, MA, RRID: SCR_001622) and presented on a 23.5-in. LCD color monitor (EIZO

FORIS FG2421) positioned 30 cm from the animal's eyes. We measured the response to red, green, and blue light with whole-screen stimulation flickering at 8.57 Hz, and with luminance varying from 2.5 cd/m^2 to the maximum provided by the monitor. Each luminance step was presented during 16.68 ms (i.e., one frame duration) followed by 100 ms of blank screen, in random order. The response was quantified as the amplitude difference between the first two ERG components (N35 and P50, see Figure 7a). Following the criteria described in Soares et al. (2010), we were able to characterize the animal as trichromats (some females) or dichromats (males and females). Dichromats were further characterized as a protanope (blind for red) or a deuteranope (blind for green). Subsequently, we obtained the ERG-based isoluminance point for the two-color pigments to which the animal was not blind. One of the colors was thereby maintained constant, while the luminance of the second color was varied in steps. For example, for a protanope monkey the color blue was fixed at 10 cd/m^2, while the green flickered over the blue at 30 Hz, from 0 to 97 cd/m^2, in 14 equidistant steps following a logarithmic scale (total of 200 repetitions for each condition). We analyzed the ERG stimulus-evoked 30 Hz oscillation response to the dichromatic stimulation using two approaches. First, by calculating the peak to valley amplitude of the ERG and determining which blue vs. green luminance pair gave rise to the lowest amplitude. These values were selected as the ones corresponding to the isoluminant point for that individual. This was confirmed by applying the Fast Fourier Transform (FFT) and selecting the luminance pair with smallest power at 30 Hz (also corresponding to the phase reversal point of the ERG stimulus-evoked oscillation). The selected luminance pair was used to construct isoluminant gratings to test for color contrast sensitivity across V2 stripes.

2.4 | Recording sessions

We used an anesthesia procedure similar to the one described above (see *Surgical procedures*), but anesthesia was maintained with a continuous intravenous infusion of fentanyl citrate (0.003 mg/kg/h) instead of isoflurane. The monkeys were immobilized with pancuronium bromide (Cristália; 0.02 mg/kg per h, *iv*) and assisted by a pressure-controlled ventilation unit (55-0798 ventilator; Harvard Apparatus, Holliston, MA). We induced cycloplegia and mydriasis with topical applications of 10% and 1% solutions of phenylephrine and tropicamide, respectively. Gas-permeable contact lenses of appropriate curvature were used to focus the eyes on a 57.3 cm distant computer screen. The positions of the blind spot and fovea were plotted onto the screen with a 180 °-reversible ophthalmoscope and stored for future analysis. The dura was accessed through a 1.5 cm^2 craniotomy using a dental drill and resected just anterior to the V1/V2 border, where we aimed to place the electrode matrix. The exposed cortex was protected with a layer of silicone oil.

2.5 | Electrodes

We used arrays consisting of varnished-coated tungsten electrodes with approximately 1 MΩ impedance at 1 kHz (FHC; Bowdoin, ME). The multielectrode matrices (~505 μm distance between closest neighbors) had slightly different configurations across our experiments

(dimensions are given in number of shanks per matrix): V202 (4 × 4 matrix in left hemisphere, 8 × 4 in right hemisphere), V204 (8 × 4 matrix in each hemisphere), and V206 (16 × 2 matrix in left hemisphere, and 8 × 4 matrix in right hemisphere). The array was positioned so that its long axis would penetrate V2 parallel to the lunate sulcus (i.e., sampling multiple V2 stripes simultaneously). Additionally, the array was tilted 10 ° anterior relative to the coronal plane in order to match the inclination of lunate's posterior bank. Electrodes in the array could not be independently moved and were thereby advanced as a single block at 200-μm steps. For each electrode, we recorded the activity of small groups of neurons (typically two or three units) for subsequent offline spike sorting. The signals were amplified and filtered between 0.7 and 5.9 kHz (HST/16o25 headset, 32-channel pre-amplifier box, Plexon, Dallas, TX, RRID:SCR_003170) before being digitized at 32 kHz by a high-speed, 16-bit resolution A/D card (PCI-6259, National Instruments, Austin, TX).

2.6 | Spike sorting

Offline cell sorting was performed using the Plexon Offline Sorter software (Plexon Inc., Dallas, TX, RRID:SCR_000012). We applied Principal Component Analysis (PCA) to reduce the number of dimensions of our correlated variables. Subsequently, spike waveforms were clustered using the *k*-means algorithm (Webb, 2002). Finally, only the well isolated units were selected manually for further analysis.

2.7 | Processing of the brain after the experiment

The animals were deeply anesthetized with 30 mg/kg (*iv*) sodium thiopental (Thiopentax™, Cristália; Itapira, SP, Brazil) and perfused intracardially before removing the brain from the skull. Perfusion was carried out using 3 L of saline (0.9%), followed by 2 L of phosphate buffer (0.1 M). V2 was subsequently flattened based on the procedure by Olavarria & Van Essen (1997). The flattened cortex was placed between two glass slides and fixated in 4% paraformaldehyde solution during 2 h. Cryoprotection was achieved by immersion in cold 5% glycerol-phosphate buffer solution during 4 h, and overnight immersion in cold 10% glycerol-phosphate buffer solution. Finally, the tissue was cut in 50 μm sections parallel to the pial surface using a cryostat and mounted on glass slides. Alternate sections were designated for Nissl (cresyl violet) staining or for CytOx histochemistry, which was performed according to the modified Silverman & Tootell (1987) method. The sections stained with cresyl violet were analyzed to determine the locations of the electrode penetration tracks. The sections reacted for CytOx histochemistry were used to reveal V2 stripes. Finally, Nissl and CytOx sections were analyzed using Photoshop CC 2015 (Adobe Systems; San José, CA, RRIC:SCR_014199) in order to align electrode penetration tracts with the localization of V2 stripes.

2.8 | Visual stimulation

Visual stimuli were generated using custom made routines in the PsychToolbox-3 package run in MATLAB. This software also sent stimulus identification codes along with onset and offset triggers to the PlexControl program in order to synchronize neuronal response

acquisition and visual stimulation. We used two different types of visual stimuli: moving bars (cases V202 and V204) and moving sinusoidal gratings (case V206). Bars consisted of 30 ° × 0.3 ° elongated stimuli of 100% contrast. They moved in one of 12 possible directions (0 °, 30 °, ..., 360 °) at a speed of 10 °/s on a 30 ° × 30 ° screen monitor. Gratings varied for the following stimulus parameters: direction and orientation of stimulus motion (0 °, 45 °, ..., 360 °), contrast (6%, 12%, 50%, and 100%), spatial frequency (0.5, 1, 2, and 4 cycles/degree or cpd), velocity (1, 3, 10, and 30 degrees/s or dps) and color (black vs. white and green vs. blue). We limited the number of stimulus combinations used in the experiments for the sake of time. Therefore, when testing for contrast we fixed spatial frequency at 1 cpd and speed at 3 dps. When testing for spatial frequency, we fixed contrast at 100% and speed at 3 dps. When testing for speed we fixed contrast at 100% and spatial frequency at 1 cpd. Black and white gratings were used in all of these previous cases. When testing for color, we set grating speed at 3 dps and spatial frequency at 1 cpd. The luminance of the two color components was set as determined by the ERG (see *Electroretinogram*). The 8 directions of motion were tested in all situations.

Receptive field mapping. We used elongated bars (see *Visual stimulation*, but 8 directions: 0 °, 45 °, ..., 360 °) to simultaneously map the center and boundaries of V2 receptive fields from neurons recorded in all electrodes from both hemispheres. This method is based on computing the latency-corrected neuronal activity in response to moving bars (Fiorani, Azzi, Soares, & Gattass, 2014). Latency imposes a delay in the neuronal response that needs to be corrected for in order to precisely estimate RF center and borders. We estimated the latency of each neuron by means of a heuristic method in which 10 empirical values, equally spaced between 20 and 120 ms, were tested. For each latency value, we created an intersected map using the responses to the eight directions of stimulus motion. The value that led to the highest response peak, corresponding to the maximal coincidence in peak response across all directions, was selected as the correction value for the latency (we used the same method to compare neuronal response latencies across V2 stripes). The half-peak of the spike density function for each of the directions of motion tested delineated a polygon, which corresponded to 50–75% of the net neuronal activity (Dow, Snyder, Vautin, & Bauer, 1981; Schiller, Finlay, & Volman, 1976). This polygon was smoothed by means of a 2D-normal convolution using a 60 ms time window (standard deviation of the Gaussian), and taken as a proxy for the RF map in the spatial domain.

2.9 | Experimental design and statistical analysis

We studied one female (V202) and two males (V204 and V206) monkeys. Neuronal activity was recorded simultaneously from multiple sites on both hemispheres (see *Electrodes* for details), which reduced possible sources of independent variability (e.g., variations in electrophysiological activity due to cortical state, external noise levels, etc.) when comparing across V2 stripes, thus improving analysis power. Our aim was to compare feature selectivity across V2 stripes based on our knowledge of V2 connectivity and previous functional work. We thereby systematically varied the following parameters of the

gratings during visual stimulation: orientation, direction, contrast, spatial frequency, speed, and color contrast (see *Visual stimulation* for details). We ran 10 repetitions (trials) of each stimulus condition. The corresponding spiking activity was aligned to stimulus onset, averaged across trials, and subsequently averaged in nonoverlapping 10 ms bins along the trial, yielding peristimulus time histograms (PSTHs). PSTHs were smoothed using a Gaussian time-window convolution filter of 60 ms, thus converting the PSTH to a spike density function (SDF). Neuronal activity for the grating stimulus was quantified by the mean firing rate within an analysis window starting 250 ms after stimulus onset (in order to exclude activity due to the stimulus onset transient) and lasting 2000 ms. Neuronal data were first submitted to the Lilliefors test of normality. Statistical comparisons between two independent data samples showing normal distributions were done using the Student's *t*-test (or the corresponding paired *t*-test for dependent samples). For corresponding non-normal distributions, we used the nonparametric Wilcoxon signed-rank. Accordingly, for comparisons involving more than two groups (e.g., orientation and direction selectivity), we used the one-way ANOVA or the Kruskal–Wallis rank sum test for normal and non-normal distributions, respectively. Tukey's post-hoc test was applied to access targeted hypothesis-driven comparisons between two sub-groups within larger samples. The threshold for statistical significance was established at alpha values below 0.05.

We accessed the direction and orientation selectivity of single units based on their responses to the gratings and single moving bars. We first accessed the neuron's selectivity to direction of motion by calculating the selectivity index (SI) as follows:

$$SI = (R_{pref} - R_{anti}) / (R_{pref} + R_{anti})$$

where R_{pref} and R_{anti} represent the activity to the preferred and anti-preferred stimulus configurations, respectively (Peterhans & von der Heydt, 1993). To compute the selectivity index for direction, the anti-preferred stimulus was defined as the one with movement direction 180 ° away from the preferred stimulus. Finally, responses were fit with parametric curves based on the probability function of the von Mises distribution, which is the circular statistics analog of the normal distribution. As proposed by Swindale, Grinvald, and Shmuel (2003), the fitting parametric curve for direction selectivity is as follows:

$$M(\varphi) = m + A_1 e^{k_1(\cos(\varphi - \varphi_1) - 1)} + A_2 e^{k_2(\cos(\varphi - \varphi_2) - 1)}$$

where φ is the grating direction of motion for which the response is being estimated, m corresponds to the baseline level, A_1 and A_2 represent the maximum heights of the individual peaks, φ_1 and φ_2 are the center directions (in radians) of each peak, and k_1 and k_2, known as concentration factors, are inversely related to the width of each peak. All parameters were adjusted by a nonlinear minimization algorithm provided in the MATLAB Curve Fitting Toolbox (The MathWorks). In addition, we pooled activities for grating stimuli with opposite directions of motion but same orientation. The antipreferred stimulus in this case was defined as the one orthogonal to the preferred stimulus. The parametric curve fitting for orientation selectivity had A_2 constrained to equal 0, which removed the second von Mises function from the equation. SI > 0.5 was the criteria used to classify a unit as selective (Peterhans & von der Heydt, 1993).

We also computed a second type of selectivity index to assess direction and orientation selectivity called circular variance for direction (CVD) or for orientation (CVO), respectively:

CVD = 1 − |Ldir|, where,

$$Ldir = \left| \frac{\sum_k R(\theta_k)\exp(i\theta_k)}{\sum_k R(\theta_k)} \right|$$

and $R(\theta_k)$ corresponds to neuronal responses to the various grating directions.

The CVO was similarly computed, except that the responses to the various axis of motion [i.e., $R(\theta_k)$] were used instead of direction in order to compute *Lori*:

$$Lori = \left| \frac{\sum_k R(\theta_k)\exp(2i\theta_k)}{\sum_k R(\theta_k)} \right|$$

CVD and CVO are known to be more robust to noise and more suitable when drawing comparisons between two different populations of responses (Mazurek, Kager, & Van Hooser, 2014). Values of CVD and CVO closer to 0 indicate stronger neuronal selectivity, while values closer to 1 indicate weaker selectivity. Values of the SI previously described follow the inverse trend.

3 | RESULTS

We simultaneously recorded the neuronal activity of multiple single-unit V2 neurons sampled across the three CytOx-defined stripes or modules of area V2, namely thick-stripe (Tk), thin-stripe (Tn), and interstripes (I-I and I-II). Recordings were performed simultaneously in

both hemispheres (2–10 ° visual eccentricity representation) of the anesthetized and paralyzed capuchin monkey (3 animals, 6 hemispheres) using multiple-electrode arrays. We used histochemical processing for the CytOx enzyme in order to assign each electrode of the array to a specific V2 stripe or module. Figure 1a-b illustrates the electrode tracks left by a 4-by-4 electrode array, which sampled one full set of V2 stripes in the right hemisphere of Animal V202. For the longer 16-by-2 array, we positioned its long axis parallel to the V1–V2 border in order to maximize sampling across the three types of V2 stripes (Figure 1c-d). In this case, we were able to simultaneously sample from up to two full sets of V2 stripes. Note that most of area V2 is buried inside the lunate sulcus. We positioned the array close to the V1–V2 border, which is located on the cortical surface. This assisted us in penetrating area V2 at an angle as perpendicular as possible to cortical surface, thereby ensuring that each electrode of the array remained within the same type of stripe along it excursion. Indeed, we did not identify any penetration that crossed between different types of V2 modules. Instances in which the electrode track could not be clearly identified, the electrode was positioned close to the border between adjacent stripes, or the CytOx histochemistry did not adequately reveal V2 bands, were excluded from our analysis. This was the case for the entire left hemisphere and some right-hemisphere electrodes in two animals (V202 and V204). We were left with 678 recording sites (sum of all recording sites shown in Table 1), from which we were able to isolate 721 single units. Subsequently, we compared the stimulus-driven and baseline activities for each single-unit using the *t*-test statistics. A total of 190 isolated neurons passed the 5% significance threshold and were thereby used for further
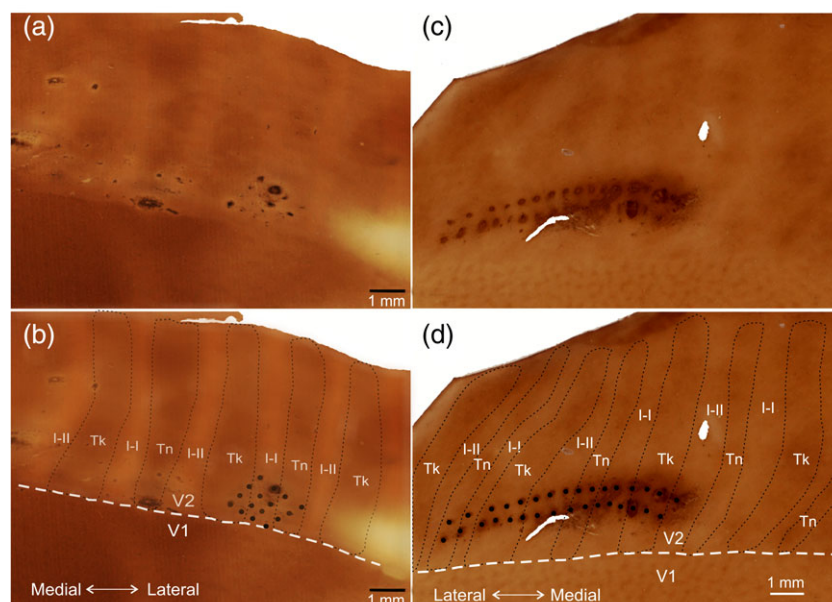

FIGURE 1 CytOx-stained sections of flattened V2 cortices showing the penetration track of the electrode matrices relative to the arrangement of the thin, thick, and interstripe V2 compartments. Top panels: original CytOx-stained histological sections; Bottom panels: original sections overlaid with black dots to indicate the individual electrode tracks; black dotted lines depict the contours of thin (Tn), thick (Th), and interstripe compartments. White dashed line shows the V1–V2 border. (a-b) 4 × 4 electrode matrix used in Animal V202 (right hemisphere). (c-d) 16 × 2 electrode matrix used in Animal V206 (left hemisphere). The interstripe compartments were further divided into I-I and I-II (see text for details). Note the CytOx-rich blobs in V1, which aid in determining the V1–V2 border (bottom panels). Scale bar = 1 mm [Color figure can be viewed at wileyonlinelibrary.com]

TABLE 1 Number of electrodes, recording sites and visually responsive single units assigned to each of the V2 stripes for the 3 animals (4 hemispheres) studied

Animal ID	Hemisphere	Electrode matrix	Electrode				Recording sites			Single units		
			Tk	I	Th	Heights	Tk	I	Th	Tk	I	Th
V202	Right	4 × 4	4	8	4	2	10	18	10	10	16	9
		8 × 4	2	2	2	1						
V204	Right	8 × 4	3	3	2	8	24	24	16	18	19	15
V206	Left	16 × 2	13	12	7	9	252	216	108	49	29	25
	Right	8 × 4	15	12	5	9						

Notes. Electrodes that could not be reliably assigned to a specific V2 stripe are not considered here. Three different configurations of electrode matrices were used during our recordings. The column heights correspond to the number of times the electrode matrix was advanced (as a single block) once it penetrated V2 cortex. Histological analysis revealed that all electrodes remained within the same V2 stripe along its entire excursion. Therefore, the column recording sites gives the total number of sites from which neuronal activity was recorded. The column *single units* depicts the number of isolated individual neurons that showed a significant level of visually driven activity relative to baseline. I = interstripe; Tk = thick-stripe; Th = thin stripe.
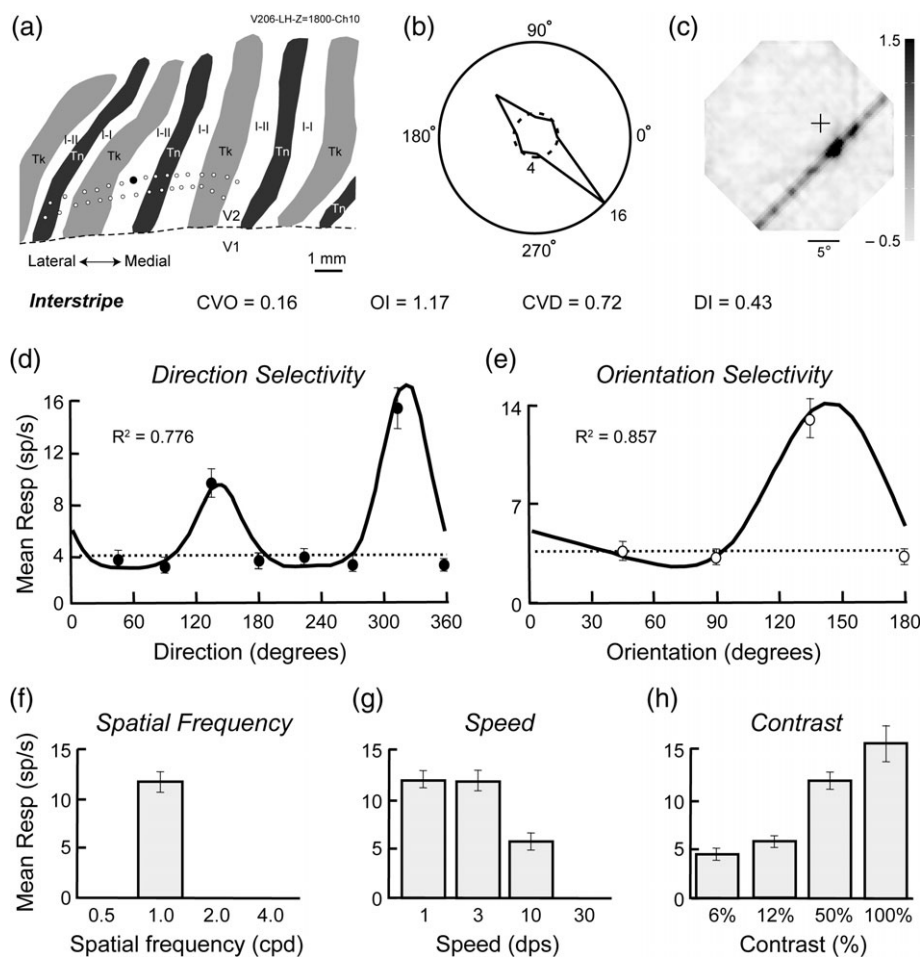

FIGURE 2 Single-unit recording illustrating the robust selectivity for stimulus orientation found in the V2 interstripe. (a) The dark dot depicts the recorded electrode within the 16 × 2 matrix (Animal V206, left hemisphere, see Figure 1d). (b) Direction tuning curve for the 100% contrast grating (1 cpd, 3 dps). Dotted and continuous circles depict the average spontaneous activity (4 spikes/s) and the maximum firing rate (16 spikes/s), respectively. Circular variance for orientation and direction (CVO and CVD, respectively), and indices for orientation and direction (OI and DI, respectively) were used to characterize the neuron's selectivity profile. (c) Automatic receptive field mapping elicited by elongated bars moving in 8 different directions. Darker shades of gray represent higher firing rates, as indicated on the gray scale to the right (in z-score units). The black cross represents the projection of the fovea on the computer monitor. Note that the RF boundaries could still be satisfactorily delineated for the nonpreferred axis of motion, despite poor neuronal response in these cases. (d) Responses to the 8 directions of motion (black dots) were fit with parametric curves based on the von Mises distribution (continuous lines, R^2 = .78, see *Method* for details). Dotted line represents spontaneous activity. (e) Analogous to (d), but the responses to grating with same orientation but opposite directions of motion were combined (R^2 = .86). The neuron did not quite reach the threshold to be classified as direction selective (DI < 0.5) and was thus classified as orientation selective (OI = 1.17). (f), (g), and (h) Response profiles to gratings of different spatial frequencies, speeds and contrasts, respectively. Full (100%) contrast gratings were used to test for spatial frequency and speed, gratings with spatial frequency of 1 cpd were used to test for speed and contrast, and gratings with speed of 3 dps were used to test for spatial frequency and contrast. Error bars depict the standard error of the mean (SEM). Scales in panel (b) are in spikes/s or sp/s

analysis. The assignment of this sub-population to each of the corresponding V2 stripes is given in Table 1.

3.1 | Example of neurons recorded in each V2 stripe

Visual stimulation consisted of moving bars (V202 and V204) and full-field gratings (V206) with different contrasts, orientations, directions of motion, spatial frequencies, velocities, and color contrasts. Figures 2–4 illustrate example neurons recorded in the interstripe, thick-stripe, and thin-stripe of area V2, respectively. Their responses illustrate the general neuronal properties characteristic of each V2 stripe, which will be summarized in the population results discussed later. Figure 2 depicts a single-unit recorded in the interstripe. It exhibits a strong orientation selectivity (Figure 2b and e) and a somewhat typical hyperbolic-type saturation curve as a function of stimulus contrast (Figure 2h). Additionally, it did not respond to the lowest spatial frequency (i.e., 0.5 cpd), nor to very highest speed (i.e., 30 dps) gratings (Figure 2f,g) we used. The thick-stripe example neuron shown in Figure 3 responded to comparatively higher grating speeds (Figure 3g) and lower spatial frequencies Figure 3f) than the interstripe neuron of Figure 2. Nevertheless, they share the feature that neuronal responses saturate for increasing grating contrasts (Figure 3h). This property sets neurons of the thin stripe apart from those recorded in thick and interstripes (Figure 4h). Note that far from

saturating, the thin stripe neuron continues to produce robust neuronal responses when grating contrast is increased to 100%. We argue that this is due to the relatively strong contribution of the parvocellular pathway to V2 thin stripe neurons. The selectivity of neurons to color contrast is not addressed in Figures 2–4. However, thin-stripe neurons in general are markedly more sensitive to color contrast than those found in thick- and interstripes, which we also argue is due to the contribution of the parvocellular pathway.

3.2 | Orientation and direction selectivity

In order to gain insight into the general neuronal properties across the 3 types of V2 stripes, we compared the population responses for orientation and direction selectivity (Figures 5 and 6), color contrast (Figure 7), contrast response function (Figure 8), spatial frequency (Figure 9), and speed (Figure 10) for the 190 single units recorded. We computed two types of indices for orientation and direction selectivity. The first consisted in the more classic measures of orientation and direction indices (OI and DI, respectively; see **Method**). In addition, we also computed more recently proposed measures of orientation and direction selectivity, as described by Mazurek et al. (2014). The latter consist in the circular variance for orientation or direction (CVO and CVD, respectively), which is arguably less sensitive to noise and more suited to comparing selectivity differences across populations. Contrary to OI
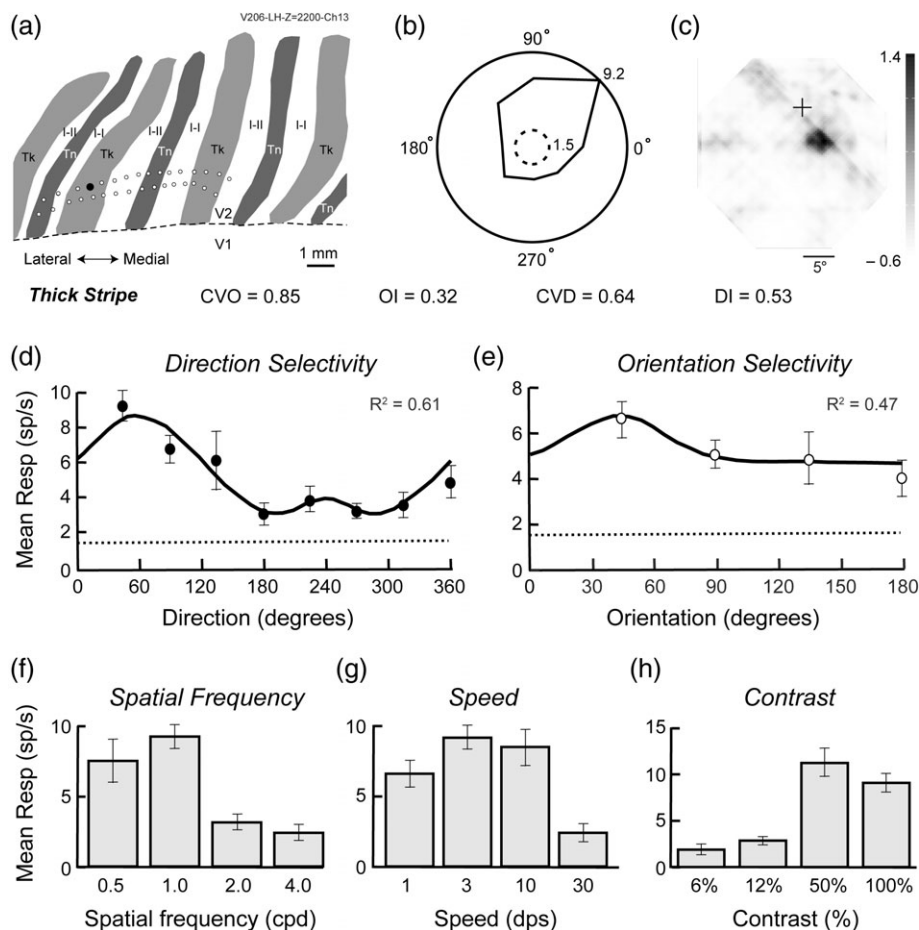

FIGURE 3 Example of a direction selective neuron recorded in a V2 thick stripe. Thick stripes come after interstripes as the V2 module with the highest percentage of direction-selective neurons. All panels follow the conventions described in Figure 2. DI > 0.5 established this unit as selective for stimulus direction. Similar to Figure 2h, note the neuronal response saturation for grating contrasts above 50%
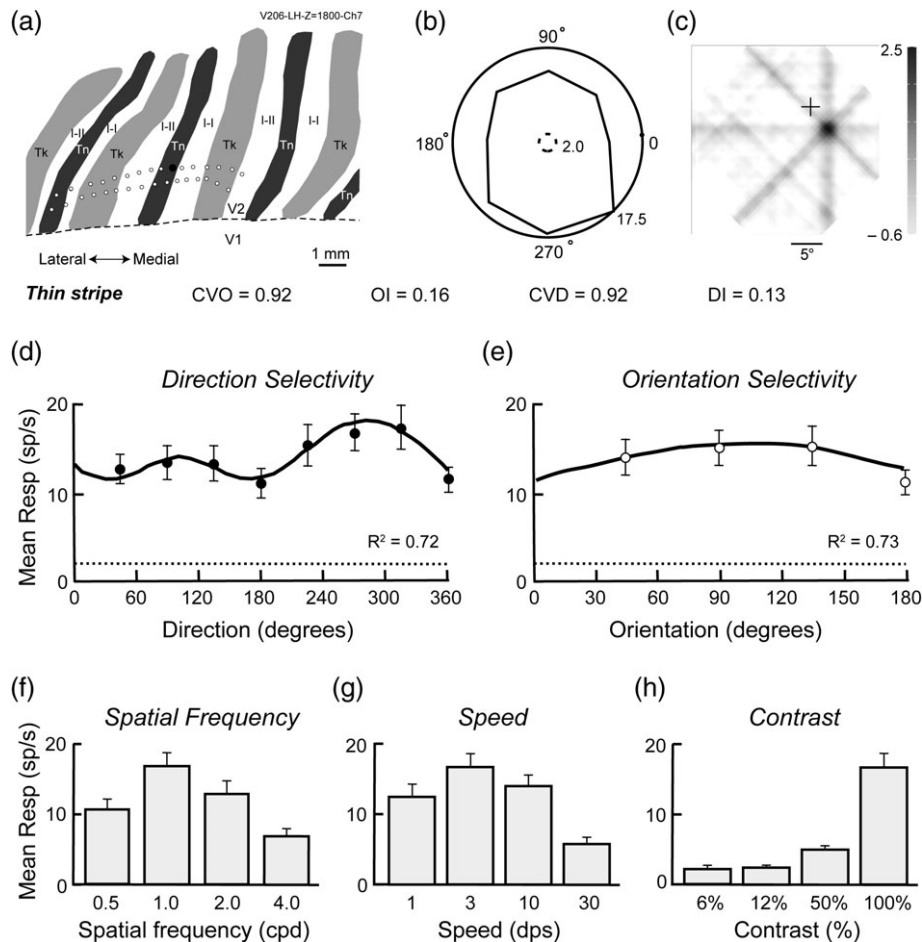
FIGURE 4 Example of a V2 thin stripe neuron exhibiting weak response saturation for contrast. All panels follow the conventions described in Figure 2. The neuron illustrated here shows poor selectivity for orientation and direction of stimulus motion

and DI, lower CVO and CVD values indicate stronger selectivity. Figure 5 summarizes the population data regarding orientation and direction selectivity using CVO and CVD (Figure 5a), and OI and DI (Figure 5b). Note that for the circular variance measures (CVO and CVD); there is no pre-established threshold that classifies the cell as either orientation or direction selective. Therefore, Figure 5a data include all 190 single units initially selected for analysis. The Kruskal–Wallis rank sum test (unbalanced) indicates that the three stripes were statistically different regarding both orientation (Kruskal–Wallis, $\chi^2 = 9.0518$, df = 2, $p = .01082$) and direction (Kruskal–Wallis, $\chi^2 = 14.422$, df = 2, $p = 7.3 \times 10^{-4}$) selectivity. Posthoc pairwise comparisons using the Tukey and Kramer (Nemenyi) test, with Tukey-distribution approximation for independent samples, indicated a significant difference between thick vs. interstripes ($p = .008$) for orientation selectivity, and between thin vs. interstripes ($p = .5 \times 10^{-3}$) for direction selectivity. The comparison thick vs. interstripes for direction selectivity did not quite reach significance ($p = .054$). The OI and DI indices, on the other hand, classically employ the 0.5 threshold in order to classify a neuron as either orientation (black bar) or direction (gray bar) selective (Figure 5b). Our analysis did not preclude classifying a neuron as simultaneously orientation and direction selective (see **Method**). However, this happened for only 28 of the 190 units (i.e., 15% of the cases). We found 39 (thick-stripe), 20 (thin-stripe), and 23 (interstripe) unclassified (i.e., nonselective) neurons within the orientation selective sub-

population, and 63 (thick-stripe), 46 (thin-stripe), and 45 (interstripe) unclassified (i.e., nonselective) neurons within the direction selective sub-population.

3.3 | Interstripe Type I vs. Type II comparison

Previous work by Shipp and Zeki (2002) indicated that interstripe Type I (I-I, lateral to thick stripes) vs. Type II (I-II, medial to thick stripes) neurons differed in their orientation selectivity. Therefore, we re-visited this issue by performing the analysis carried out in Figure 5, but specifically comparing units recorded in Type I vs. Type II interstripes (Figure 6). Wilcoxon signed-rank test indicated no statistical difference for direction selectivity ($p = .634$, $Z = .4758$), and only a near-significant difference for orientation selectivity ($p = .069$, $Z = 1.8216$). Therefore, we assume Type I and II interstripe neurons to have homogeneous neuronal properties regarding orientation and direction tuning.

3.4 | Color sensitivity

Analysis of color-coding was one property that set thin-stripe neurons apart from those in the thick and interstripe. Male capuchin monkeys are typically dichromates (Soares et al., 2010). To study color-contrast sensitivity in one of our male subjects (V206), we carried out an
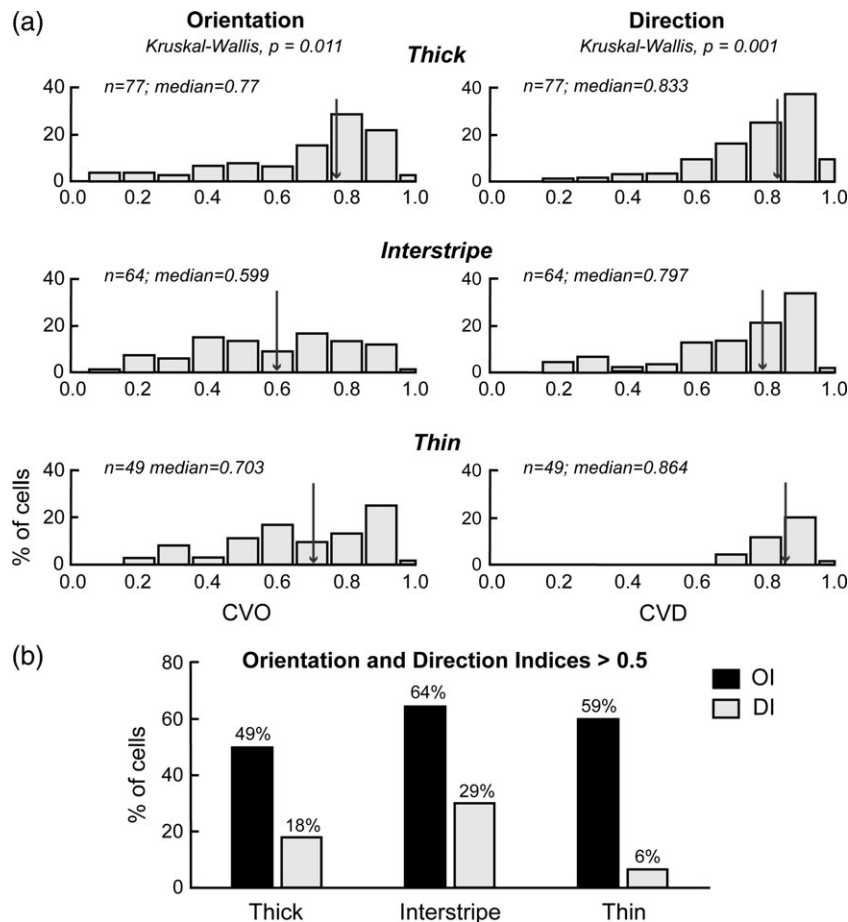
FIGURE 5 Population data indicate that neurons in thick, thin, and interstripe of V2 exhibit different levels of selectivity for orientation and direction of stimulus motion. (a) Interstripes exhibited the strongest orientation and direction selectivity, as evidenced by the respectively lower CVO and CVD medians (depicted by arrows) estimated for this neuronal population. Thin stripes showed the second-strongest orientation selectivity profile, followed by thick stripes. On the other hand, thick stripe neurons showed stronger direction selectivity compared to thin stripes. Gratings were used as visual stimuli (100% contrast, 1 cpd, 3 dps). (b) Similar analysis to (a), but adopting the more traditional orientation and direction indices (OI and DI, respectively) used in the literature, enabling comparison with previous published work. Note that the selectivity estimates obtained using CVO (CVD) are compatible with those adopting OI (DI) for all V2 modules

electroretinogram (ERG, see **Method**) to identify which two of the three cone types (i.e., red, green and blue) were present in this particular individual. We thereby presented full-field red, green, or blue stimulus that flickered at various luminance levels and measured the corresponding amplitude of the N35-P50 component in the ERG (Figure 7a). The observation that the ERG response amplitude was unusually low and remained low for increasing luminance levels of the red flicker stimulus indicated a deficiency of the red cone, which led us to classify this individual as a protanope (deficient for red). We subsequently determined the isoluminant point for the two types of cones present in this individual (i.e., green and blue) by measuring the ERG response to flicker stimulation (see **Method**). These values were used to construct isoluminant green-blue gratings in order to establish the proportion of neurons across the different V2 stripes that were sensitive to color contrast. We used the subpopulation of 103 single units from Animal V206 for this analysis. Our criteria consisted in comparing baseline vs. isoluminant grating responses using the Student's t-test. Figure 7b shows that the thin stripe contains the largest proportion of color-contrast sensitive neurons (80%), followed by the thick stripe (47%) and the interstripe (21%). Additionally, we

computed the corresponding neuronal population response measured in each of the V2 stripes to isoluminant gratings and compared it to baseline (Figure 7c). The response of thin-stripe neurons to color stimuli was 153% greater than baseline, while the corresponding increases in activity for thick and interstripe neurons were approximately 3-fold lower (58% and 51%, respectively). One of our aims was to investigate the extent to which color processing is segregated from form processing in area V2. We thereby investigated the orientation and direction selectivity of the subpopulation of color-selective neurons derived from all three types of V2 stripes combined (N = 49, depicted in Figure 7b). Figure 7d and e show measures of orientation and direction selectivity expressed by means of the CVO/CVD or OI/DI. Surprisingly, 86% of the color-selective cells were also orientation selective, indicating that color and form processing in area V2 are intimately associated. This proportion is higher than the ones reported by Levitt et al. (1994) and Gegenfurtner et al. (1996).

3.5 | Contrast response curve

The second property that sets thin-stripes neurons apart from those found in thick- and interstripes concerns the shape of their
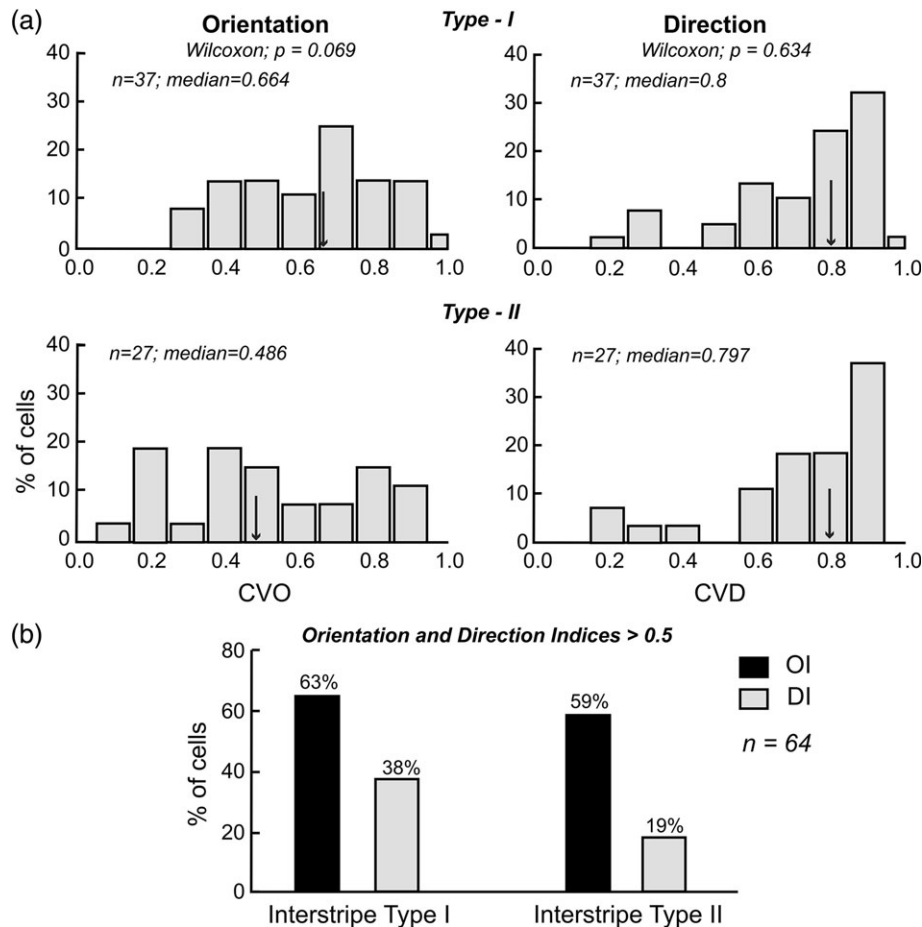
FIGURE 6 Selectivity differences between Type I and Type II interstripes. (a) Interstripe Type II neurons show a trend for stronger orientation selectivity compared to Type I (left panels). Practically no difference is observed for direction selectivity (right panels). (b) Similar analysis to (a), adopting the orientation and direction indices (OI and DI, respectively; see legend for Figure 5). Description of visual stimuli used as in Figure 5

corresponding contrast response curves. We computed the population data using both the absolute (Figure 8a) and the normalized (Figure 8b) neuronal responses as a function of grating contrast. Typically, visual responses show a gradual saturation with increasing stimulus intensity. This behavior can be described by a hyperbolic function and is best exemplified by the responses of thick-stripe neurons as grating contrast reaches 100% (Figure 8a). Thin-stripe neurons, on the other hand, show no evidence of saturation and continue to linearly increase their responses until up to 100% contrast. The responses to the 100% contrast grating were statistically different between neurons in the thin vs. thick and interstripes ($p = .0162$, $Z = 2.4038$), as measured using the Wilcoxon rank sum test. Quantitatively, the C_{50} (contrast at which half of the maximum response is reached) for thick-stripe neurons was nearly half (27%) the one observed for thin-stripe neurons (48%), while the corresponding R_{max} (maximum response) was 6.17 sp/s and 9.85 sp/s, respectively. Interstripe neurons showed a somewhat intermediate behavior, albeit much more similar to thick-stripe neurons. The slow response saturation of thin-stripe neurons is less evident when neuronal responses are normalized before averaging (Figure 8b), mainly due to the fact that the normalization procedure is based on the minimum and maximum response values.

However, here we can better observe that thick stripe neurons are more sensitive to small variations in contrast at lower stimulus intensities and gradually saturate their responses at higher contrasts levels. The opposite is true for thin stripe neurons. These results favor the notion that thick-stripe neurons receive a relatively stronger input from the magnocellular pathway, while the parvocellular pathway projects preferentially to the thin stripe. The fact that thin stripe neurons are more sensitive to color-contrast (Figure 7b,c) corroborates this notion.

3.6 | Selectivity to stimulus spatial frequency

We used four different gratings (0.5, 1.0, 2.0 and 4.0 cpd) to test the spatial frequency selectivity of neurons across V2 stripes (Animal V206). We computed the population data using both the absolute (Figure 9a) and the normalized (Figure 9b) neuronal responses as a function of grating spatial frequency. Note that the non-normalized responses of thin-stripes neurons are overall higher than those measured for thick-stripe and interstripe neurons (Figure 9a). This can be explained by the fact that we used 100% contrast gratings in these experiments and that thin-stripe neurons show slow saturation to stimulus contrast (Figure 8). The primary conclusion that can be taken from
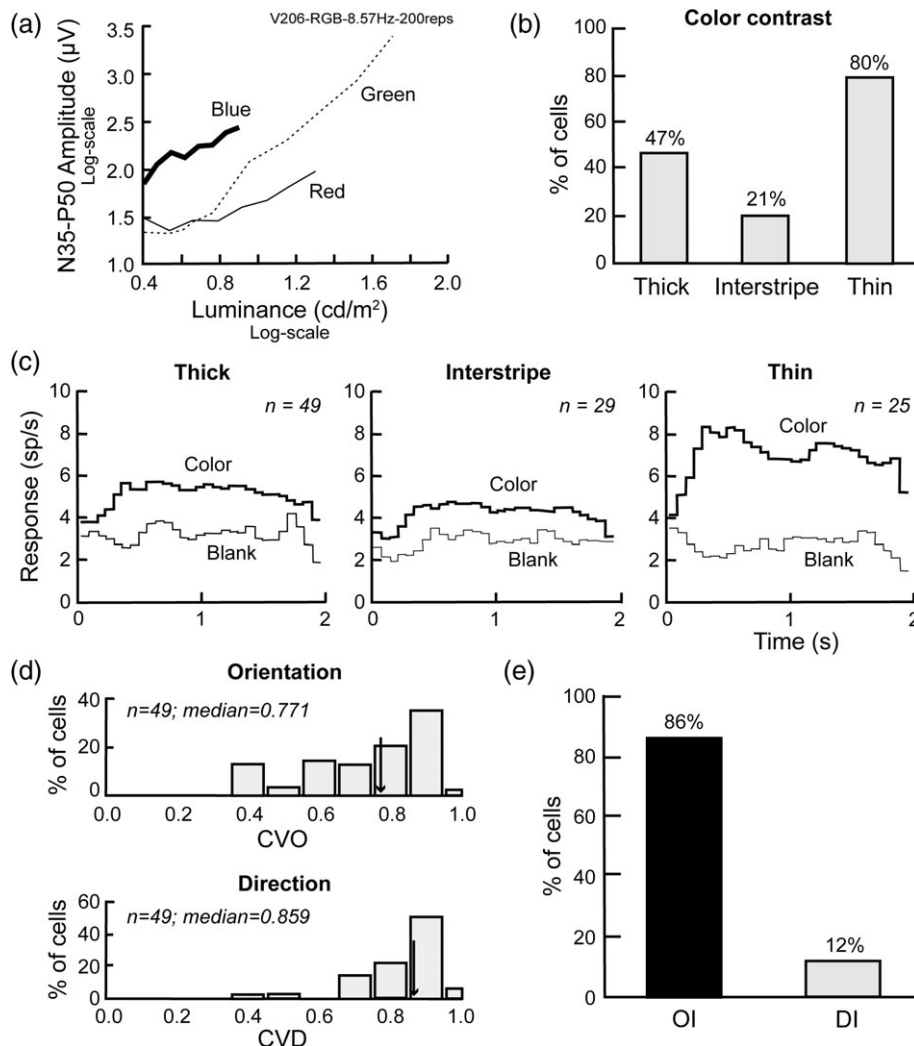
FIGURE 7 Thin stripes are the V2 modules containing the highest proportion of color-contrast sensitive neurons. (a) The electroretinogram (ERG) N35-P50 peak-to-trough amplitude measured as a function of luminance intensity for the blue, green and red stimuli. Note the diminished response to red, compared to blue and green, as luminance increases. This individual was thus classified as a protanope (absence of red cones). The ERG also enabled us to determine the isoluminance levels for blue and green (data not shown), which were used to construct the color gratings employed in subsequent experiments. (b) Thin stripes contained a substantially higher proportion of neurons (80%) that were responsive to color contrast compared to the thick and interstripes (47% and 21%, respectively). (c) Thin stripe neurons also responded more vigorously to color contrast compared to thick and interstripes, as shown by the population response to the blue-green isoluminant gratings. Responses to the blank screen, equivalent among the three stripes, are also illustrated. (d) Orientation and direction selectivity profile of all neurons sensitive to color-contrast recorded in thick, thin, and interstripes combined (N = 49), as measured using CVO and CVD. (e) Similar analysis to (d), adopting the orientation and direction indices (OI and DI, respectively). Note that a high proportion of the color-contrast sensitive neurons are also orientation selective. Gratings with 1 cpd moving at 3 dps were used as visual stimuli

the normalized responses shown in Figure 9b is that neurons across all stripes show a very similar selectivity profile to spatial frequency. Ideally, we would have tested a more extensive set of spatial frequencies in order to obtain a finer sample of spatial frequency preference. Unfortunately, our experimental design already contained a large number of conditions and we were concerned that testing additional spatial frequencies might lead to prohibitively long recording sessions. In order to estimate the preferred spatial frequency of neurons in each stripe using a limited set of four data points, we calculated the percentage of neurons preferring each one of the four spatial frequencies and subsequently computed the geometric mean (gmean) across the percentages. Therefore, the gmean was based on the preferred spatial frequency value for each unit. Figure 9c shows the corresponding percentages

and gmeans across the three types of V2 stripes. The gmean results are consistent with those of the average population activity in Figure 9a,b, namely that interstripe neurons prefer higher spatial frequencies, while thick-stripe neurons prefer lower spatial frequencies. Thin-stripe neurons assume an intermediate behavior.

3.7 | Selectivity to stimulus speed

Similar to the experiments on spatial frequency preference, we also compared neuronal selectivity to stimulus speed (1, 3, 10, and 30 dps), across V2 stripes, in animal V206 (Figure 10). Here, we also used 100% contrast gratings, which explains the overall response offset evident for thin-stripe neurons (Figure 10a; compare with Figure 9a). As justified
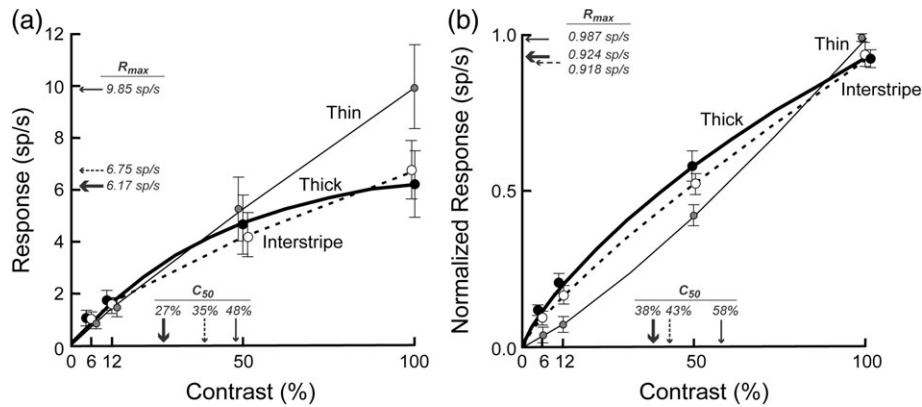
FIGURE 8 Thin stripe neurons exhibit slow saturation to stimulus contrast when compared to neurons in the thick and interstripes. (a) Contrast response curves to gratings (1 cpd, 3 dps, and optimal direction of motion) for the thick (thick line, $N = 49$), thin (thin line, $N = 25$), and interstripe (dashed line, $N = 29$) neuronal populations obtained by averaging the absolute (non-normalized) firing rates. Contrast values of 6%, 12%, 50%, and 100% were used. The C_{50} value (contrast at which half of maximum response is reached) for the thin stripe is higher (48%) compared to the thick and interstripes (27% and 35%, respectively), which indicates a slower saturation of the neuronal response to increasing contrast values. Accordingly, the maximum response (R_{max}) was higher for thin stripes (9.85 sp/s) compared to thick and interstripes (6.17 sp/s and 6.75 sp/s, respectively). (b) Same as in (a), but the neuronal responses were normalized before averaging. The R^2 for all hyperbolic fits reached values above 0.99. Error bars depict the standard error of the mean. The mean data points and the corresponding SEMs in both panels are slightly displaced horizontally to aid visualization

above, the normalized neuronal responses in this case are more informative when comparing speed selectivity across V2 stripes (Figure 10b). As with spatial frequency, neuronal selectivity for stimulus speed was somewhat similar across our population. Neurons in the three stripes preferred velocities around 3 dps, with peak values ranging between 1 and 10 dps. However, compared to thin and interstripes, thick-stripe neurons responded significantly weaker to the lowest stimulus velocity used (comparison thick-stripe vs. thin and interstripe neuronal responses to 1 dps, Wilcoxon signed-rank test, $p = 4.4 \times 10{-16}$, $Z = -8.1204$). Additional insight into the relative tuning for stimulus velocity across V2 stripes is given in Figure 10c. As in Figure 9c, we computed the gmean across the percentage of neurons preferring each of the four speeds tested. Comparatively, thick-stripe neurons showed preference to higher speed stimuli, followed by interstripe and thin-stripe neurons (gmeans = 2.90, 2.32, and 2.21, respectively).

3.8 | Latency of the neuronal responses

V2 stripes receive different contributions from the magno- and parvocellular visual pathways (Livingstone & Hubel, 1984,1987), as well as a heterogeneous set of feedback projections from hierarchically superior visual areas (Nascimento-Silva et al., 2014). Distinct pathways have been associated with different conduction speeds of neuronal information, which could potentially influence neuronal response latency across V2 stripes. Therefore, we set out to test if neurons across the thick, thin, and interstripes showed any difference in their response latency. Results in Figure 11 are based on responses to moving bars (Animals V202 and V204) and to moving gratings (Animal V206). Neurons in the interstripe showed the shortest response latency (80 ms), followed by neurons in the thin-stripe and thick-stripe (both with 90 ms). However, these differences were not statistically significant (Kruskal–Wallis, $\chi^2 = 4.3593$, df = 2, $p = .1131$), showing that the differences in stimulus selectivity and functional connectivity across V2 stripes are not reflected in the response latency of neurons.

4 | DISCUSSION

Here, we investigate the functional specialization of the CytOx-characterized macro-modules of area V2. V2 constitutes a nodal point within the visual hierarchy, where the dorsal and the ventral pathways of visual information processing diverge (Ungerleider & Mishkin, 1982). Therefore, understanding the functional specialization of V2 modules is key to elucidating parallel processing in the early and intermediate visual systems. Our work presents several advances relative to previous publications on this topic. We used multielectrode arrays to simultaneously record neuronal activity on both hemispheres, which reduced possible sources of independent variability (e.g., variations in electrophysiological activity due to cortical state, external noise levels, etc.). We present robust CytOx histochemistry, associated with flat-mount preparations of area V2, in order to localize each of our multiple eletrode matrices within the V2 compartments. Our analysis is based on carefully isolated single-unit activity, while most of the previous publications is based on multiunit activity. Economides, Sincich, Adams, & Horton (2011) have shown that multiunit recordings may yield low accuracy orientation and direction selectivity data due to the possibility that the neuronal ensemble being acquired exhibits distinct preferences. Additionally, we use circular variance analysis to estimate the orientation and direction selectivity of V2 neurons (CVO and CVD, respectively). Mazurek et al. (2014) showed that CVO and CVD yield more precise estimates of orientation and direction selectivity, are less prone to noise and are better suited to analyze population data, as compared to the classic orientation and direction selectivity indices (OI and DI, respectively; see Peterhans & von der Heydt, 1993). We carry out a systematic investigation of speed tuning across V2 stripes, a stimulus feature somewhat neglected in previous work. Finally, we present the first study of this sort in the capuchin monkey, which is a New-World diurnal monkey with brain size and sulcal pattern similar to that of *Macaca fascicularis*.
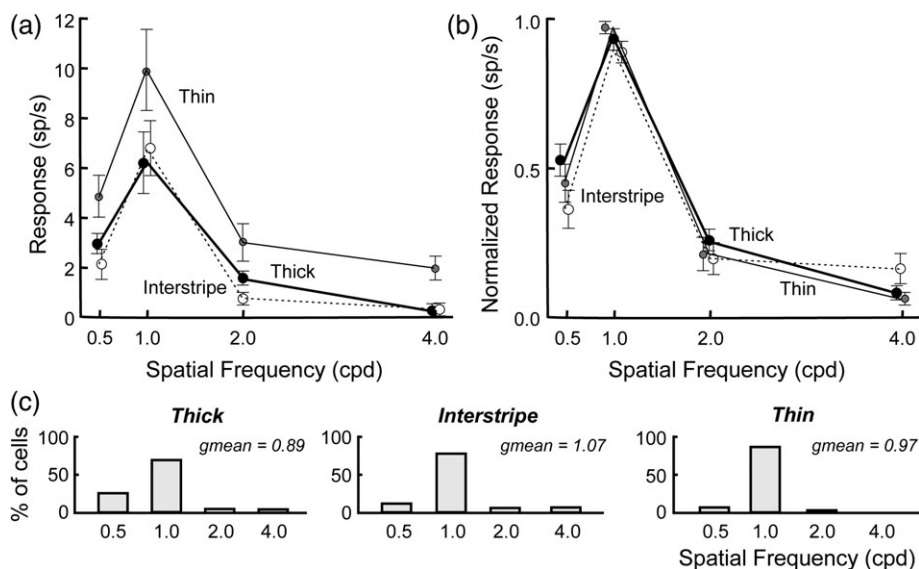
FIGURE 9 Thick stripe neurons respond best to lower, while interstripe neurons prefer comparatively higher spatial frequencies. (a) Neuronal activity as a function of spatial frequency (0.5, 1, 2, and 4 cpd) for the thick (thick line, N = 49), thin (thin line, N = 25) and interstripe (dashed line, N = 29) neuronal populations obtained by averaging the absolute (non-normalized) firing rates in response to 100% contrast gratings (3 dps, optimal direction of motion). Most neurons responded optimally to spatial frequencies between 0.5 and 2 cpd. Note that thin stripes expressed an overall higher firing rate compared to the two other stripes (see *Results* for details). (b) Same as in (a), but the neuronal responses were normalized before averaging, which removed the response offset for thin stripe neurons. This procedure corroborates the notion that low and high spatial frequency stimuli preferentially activate thick and intestripe neurons, respectively. (c) Percentage of neurons showing preference to each of the four spatial frequencies tested. Overall tendency of the population is expressed in the form of the geometric mean (gmean). Error bars in (a) and (b) depict the standard error of the mean

In accordance with previous studies, we found that neurons across the three stripes have a substantial overlap in their response properties. Examples of stimulus features that are similarly coded across stripes include spatial frequency and velocity, albeit with some reliable differences. For example, thick stripe neurons yield comparatively poor responses to low stimulus speed, as expected by the contribution they receive from the magnocellular pathway. The latency of the neuronal responses to visual stimulation was also statistically indistinguishable
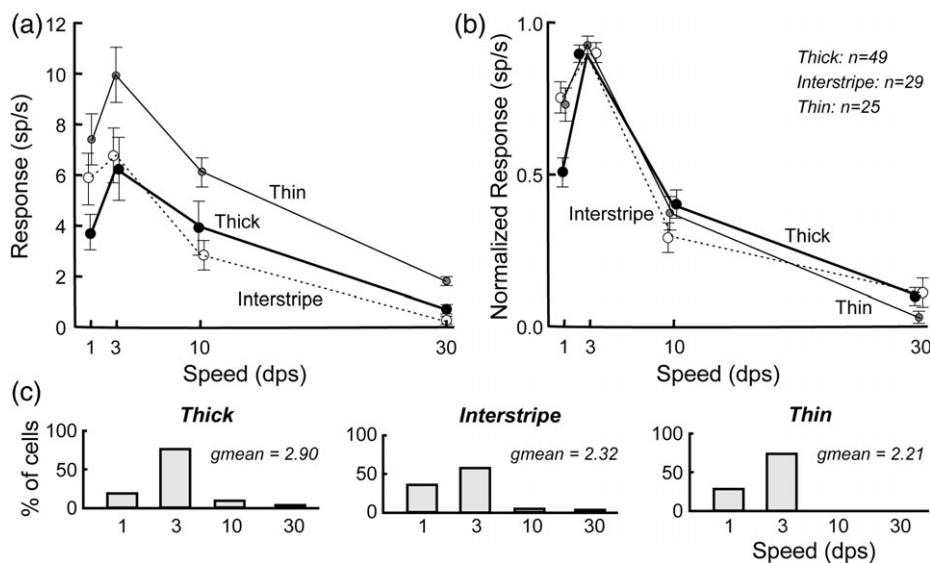

FIGURE 10 Thin and interstripe neurons prefer low-velocity stimulus, while thick-stripe neurons prefer velocities that are comparatively higher. (a) Neuronal activity as a function of stimulus velocity (1, 3, 10, and 30 dps) for the thick (thick line, N = 49), thin (thin line, N = 25) and interstripe (dashed line, N = 29) neuronal populations obtained by averaging the absolute (non-normalized) firing rates in response to 100% contrast gratings (1 cpd, optimal direction of motion). Most neurons responded optimally to stimulus velocities between 1 and 10 dps. Note that (as observed for spatial frequency) thin stripes expressed an overall higher firing rate compared to the two other stripes. (b) Same as in (a), but the neuronal responses were normalized before averaging, which removed the response offset for thin stripe neurons. This procedure corroborates the notion that thick and thin stripe neurons respond relatively poor to low and high velocity stimuli, respectively. (c) Percentage of neurons showing preference to each of the four stimulus velocities tested. Overall tendency of the population is expressed in the form of the geometric mean (gmean). Error bars in (a) and (b) depict the standard error of the mean
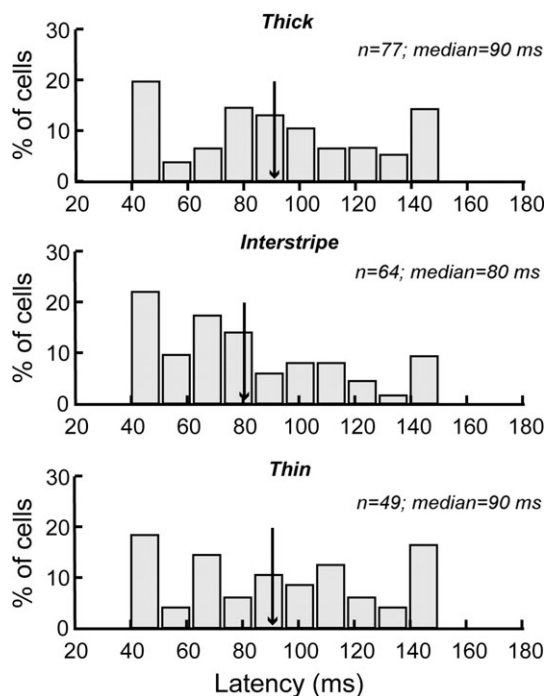
FIGURE 11 Response latency is not significantly different across V2 stripes. Moving bars (100% contrast, 10 dps) and gratings (100% contrast, 1 cpd, 3 dps) were used as visual stimuli. Latencies were grouped in 10 ms bins distributed between 40 and 150 ms. Arrows indicate the population median, also depicted at the top of each panel, along with the number of neurons recorded in each stripe. Medians did not differ statistically from each other ($p > .05$, Kruskal–Wallis test, unbalanced data)

across stripes. However, we found some consistent functional specializations. Color contrast was best coded by thin stripe neurons (a finding that is in accordance with previous works), while orientation and direction selectivity were best coded by interstripe neurons (still a controversial issue in the literature). A large proportion (86%) of neurons across all stripes that responded to color were found to be also selective to stimulus orientation, showing that area V2 already contains highly integrated information regarding the various features of the visual stimulus. Finally, thin stripe neurons were the ones showing the slowest response saturation to increasing stimulus contrast, while thick stripe neurons exhibited the fastest saturation.

4.1 | Contrast sensitivity and selectivity to other stimulus features

One of our most important findings was that thin stripe neurons showed no sign of response saturation at the high contrast range (i.e., > 50%), while thick stripe neurons had already reached the asymptotic phase of the hyperbolic contrast-response curve (see Figure 8). Few electropysiological studies have investigated the sensitivity to contrast across V2 stripes. Levitt et al. (1994) found thin stripe neurons to be significantly less sensitive than those found in thick and interstripes, while the latter two did not significantly differ from one another. Lu and Roe (2007) used the intrinsic signal optical imaging technique to examine contrast responses at different V2 functional domains. They report that while the hemodynamic signal at

thick and interstripes saturate, the signal measured at the thin stripes continues to increase at high-contrast levels. These data suggest a strong influence of the inputs from the parvocellular pathway to the thin stripes in V2, which is assumed to be responsible for the processing of color and brightness information.

The degree to which neurons in the three V2 compartments are selective for the orientation and direction of the stimulus has been more extensively investigated. Previous works agree that interstripe neurons show the highest selectivity for orientation compared to those in the thick and thin stripes (DeYoe & Van Essen, 1985; Peterhans & von der Heydt, 1993; Levitt et al., 1994; Munk, Nowak, Girard, Chounlamountri, & Bullier, 1995; Roe & Tso, 1995; Gegenfurtner et al., 1996; Tamura et al., 1996; Yoshioka & Dow, 1996; Shipp & Zeki, 2002). Data for direction selectivity are more contradictory in the literature. We found interstripe neurons to show the strongest direction selectivity, which is in accordance with Peterhans & von der Heydt (1993) and Tamura et al. (1996). On the other hand, DeYoe & Van Essen (1995), Levitt et al. (1994), Gegenfurtner et al. (1996), and Shipp & Zeki (2002) all found thick stripe neurons to be the most direction selective. It is important to point out that only Levitt et al. (1994) and Tamura et al. (1996) analyzed single units, while the other published works analyzed multiunit activity. As noted above, this may yield imprecise estimations of orientation and direction selectivity. Additionally, the data described by Levitt et al. (1994) did not reach statistical significance. Therefore, a surprising result in our work was that thin stripes contained a higher percentage of orientation selective neurons compared to thick stripes, and that both stripes contained a comparable percentage of direction selective neurons (see Figure 5).

In accordance with previous studies (DeYoe & Van Essen, 1985; Gegenfurtner et al., 1996; Tamura et al., 1996), our work shows that thin stripes contain by far the largest proportion of neurons responding to color. This result is consistent with the strong contribution that the thin stripe receives from the parvocellular pathway (Livingstone & Hubel, 1984, 1988). However, there is controversy regarding the second most color-sensitive stripe. We found it to be thick stripes, followed by interstripes, which is in agreement with Roe and Tso (1995), Gegenfurtner et al. (1996) and Shipp & Zeki (2002). On the other hand, DeYoe & Van Essen (1985) and Levitt et al. (1994) found it to be interstripes, followed by thick stripes. It is thereby curious that interstripe neurons respond well to some stimulus parameters that are related to object discrimination (e.g., orientation), but poorly to others (e.g., color). Regardless of this finding, our data show that the integration of color and orientation is already accomplished in V2, because 86% of the neurons that respond to color were also orientation selective. This is in accordance with Leventhal, Thompson, Liu, Zhou, and Ault (1995) and Friedman, Zhou, and von der Heydt (2003), but in direct contradiction with the classical work by Livingstone & Hubel (1984), who proposed that cells up to V2 would not integrate color information and border detection. Our findings are consistent with Johnson, Hawken, & Shapley (2008), who showed that orientation and color information are already integrated in upstream area V1 (for review, see Shapley & Hawken, 2011).

4.2 | Latency of neuronal responses across stripes

The parvocellular and magnocellular pathways provide differential contributions to the various V2 stripes (Livingstone & Hubel, 1984,1988). Since these two pathways are associated with different response latencies to visual stimulation (Nowak et al., 1995), we also expected the response latencies across stripes to differ from each other. The response latencies of thick and thin stripes were indistinguishable. Interstripe neurons did show faster responses, but they were also statistically indistinguishable from those recorded in the thick and thin stripes. Our results are in disagreement with Munk et al. (1995), who showed that thick and interstripe neurons exhibit a response latency, which is in average 20 ms shorter compared to thin stripes. A possible reason for this discrepancy may be due to the method used to compute response latency. Our analysis was based on the peak response to visual stimulation, while the analysis by Munk et al. (1995) was based on the latency of the first spikes after stimulus onset.

4.3 | Visual responsiveness of V2 neurons

We observed a relatively low proportion of visually responsive neurons in V2 (190 stimulus-driven neurons out of 721 isolated single units). We have a few possible explanations for this. First, we performed a fully unbiased recording, meaning that we positioned the electrode matrix in V2 without any feedback of the corresponding neuronal activity and if the recording sites showed visually-driven responses. This was in part because we used a multieletrode matrix that moved as a block (see Method). Optimizing the recording position for each individual electrode was not possible. On the other hand, our approach enabled an unbiased assessment of the proportion of visually-driven neurons in V2 (at least for the visual stimuli we employed). Second, we did not optimize the properties of the stimulus for each recording site, something that is also impractical with multi-electrode recordings. This includes the property of stimulus size. For example, Levitt et al. (1994) optimized the size of the stimulus as a function of receptive field size, which may have contributed to their finding of a higher incidence of visually responsive neurons in V2. Moreover, we used simplified visual stimuli (bars and gratings) in our experiments, while others have demonstrated that V2 responds more vigorously to complex and naturalistic visual stimuli (Hegde & Van Essen, 2000; Freeman, Ziemba, Heeger, Simoncelli, & Movshon, 2013). However, our experimental design required that we used a simplified visual stimulus (gratings), where we could easily parameterize properties such as contrast, spatial frequency and speed in order to compare neuronal selectivity across V2 stripes.

4.4 | Receptive field structure across V2 stripes

Our work did not investigate differences in receptive field structure across V2 stripes. This was mainly due to our choice of the visual stimuli employed during the experiments. We opted for elongated bars and full-field gratings that could simultaneously stimulate the receptive fields of all sites being recorded. With our experimental design, it would have been impractical to investigate in detail the receptive field structure of all neurons being recorded. The elongated bars we used

for mapping provided us with a first comparative insight into V2 receptive field structure (namely receptive field center and size) across V2 stripes. However, the moving bars we employed provide a rather limited assessment of receptive field size (Fiorani et al., 2014), which could provide valuable information on the visual acuity across stripes. They do provide, on the other hand, a very accurate estimation of receptive field center. Examining the fine architecture of individual V2 receptive fields would require lengthier experiments and the use of more spatially-restricted (and often more complex) visual stimuli. Future work using a different experimental design will be necessary to further address this issue. However, they will probably rely on a more restricted number of electrodes, which would limit the number of V2 sites being simultaneously investigated.

4.5 | Comparison of V2 stripes across New and Old-World monkeys

The morphological parameters of V2 stripes in the capuchin monkey (width, length, and total number of stripes) are strikingly similar to those described in the macaque (Nascimento-Silva et al., 2014). Additionally, we found that the V2 stripes in the capuchin monkey cortex are orthogonally disposed relative to the V1/V2 border and that they extend all the way from the central to the peripheral representation of the visual field (Rosa et al., 1988), as has been described in the macaque (Tootell, Silverman, De Valois, & Jacobs, 1983). Our group has carried out extensive work on the cortical organization and connectivity of the visual cortex in both species. The pattern of V2 projections to its main cortical targets, namely areas V3, V4, MT, PO, VIP and LIP, are very similar in the capuchin and macaque monkeys (Gattass et al., 1997; Gattass, Lima, Soares, & Ungerleider, 2015). V2 subcortical projections in both monkeys are also alike, with the exception that V2 projects to the P1 and P2 regions of the pulvinar thalamic nucleus in the macaque (Ungerleider, Galkin, Desimone, & Gattass, 2014), while V2 projects only to P1 in the capuchin (Gattass, Soares, & Lima, 2018). Therefore, our morphological, anatomical and connectivity studies do not predict any fundamental difference in the functional organization of V2 stripes between capuchin and macaque monkeys. Indeed, the discrepancies between our work and those published on the macaque are not in any way more pronounced than the discrepancies among the latter. Future work should address if the differences in color vision between New and Old-World monkeys impact the functional organization of V2 stripes. Macaques and some female capuchin monkeys are trichromats, while normal male capuchin monkeys are dichromats (Soares et al., 2010). It would be interesting to specifically investigate color sensitivity differences in the thin stripe between dichromat versus trichromat capuchin monkeys. This could reveal important organizational aspects of the color processing machinery when an additional opsin is present in the retina.

4.6 | Segregation and integration of stimulus information processing across V2 stripes

Several publications have supported the notion that information processing is segregated across V2 stripes (DeYoe & Van Essen, 1985,1988; Hubel & Livinstone, 1985; Livingstone & Hubel, 1984;

Roe & Tso, 1995; Shipp & Zeki, 1985,1989; Zeki & Shipp, 1988). Our results, on the contrary, support a substantial integration of several stimulus features within the same V2 stripe, a view that has been corroborated by others (Gegenfurtner et al., 1996; Kiper et al., 1997; Levitt et al., 1994; Shipp & Zeki, 2002; Tamura et al., 1996). Indeed, Economides et al. (2011) have recently shown that the V1 modules that differently project to V2 stripes, namely the patches and interpatches, already share similar stimulus selectivity properties (e.g., orientation selectivity). Shipp & Zeki (2002) reported that the clearest functional segregation across stripes can be observed in Layer III of V2. Unfortunately, we were unable to ascertain the cortical layer in which each probe of our multielectrode array was located. Due to the complexity and technical challenges of thoroughly describing the properties of V2 stripe neurons, further work will be required to revisit this issue until a broader consensus can be reached.

CONFLICT OF INTEREST

We declare no conflict of interest.

IN MEMORIAM OF VIVIEN ALICE CASAGRANDE

Vivien Casagrande made fundamental contributions to the understanding of cortical organization of primates. Her great enthusiasm, superb scientific expertise and rigorous application of neuroanatomical techniques has greatly influenced this field of research. For us, she will be missed!

AUTHOR CONTRIBUTION

R.P., J.G.M.S., B.L., R.G. designed research; R.P., J.G.M.S., B.L., M.C., M.F., R.G. performed research; R.P., B.L. analyzed data; R.P., J.G.M.S., B.L., R.G. wrote the paper.

ORCID

Bruss Lima https://orcid.org/0000-0001-6865-2900
Ricardo Gattass https://orcid.org/0000-0002-0321-1490

REFERENCES

Brainard, D. H. (1997). The Psychophysics Toolbox. *Spatial Vision*, *10*, 433–436.

Carroll, E. W., & Wong-Riley, M. T. (1984). Quantitative light and electron microscopic analysis of cytochrome oxidase-rich zones in the striate cortex of the squirrel monkey. *Journal of Comparative Neurology*, *222*, 1–17.

DeYoe, E. A., & Van Essen, D. C. (1985). Segregation of efferent connections and receptive field properties in visual area V2 of the macaque. *Nature*, *317*, 58–61.

DeYoe, E. A., & Van Essen, D. C. (1988). Concurrent processing streams in monkey visual cortex. *Trends in Neuroscience*, *11*, 219–226.

Dow, B. M., Snyder, A. Z., Vautin, R. G., & Bauer, R. (1981). Magnification factor and receptive field size in foveal striate cortex of the monkey. *Experimental Brain Research*, *44*, 213–328.

Economides, J. R., Sincich, L. C., Adams, D. L., & Horton, J. C. (2011). Orientation tuning of cytochrome oxidase patches in macaque primary visual cortex. *Nature Neuroscience*, *14*, 1574–1580.

Federer, F., Ichida, J. M., Jeffs, J., Schiessl, I., McLoughlin, N., & Angelucci, A. (2009). Four projection streams from primate V1 to the cytochrome oxidase stripes of V2. *The Journal of Neuroscience*, *29*, 15455–15471.

Federer, F., Williams, D., Ichida, J. M., Merlin, S., & Angelucci, A. (2013). Two projection streams from macaque V1 to the pale cytochrome oxidase stripes of V2. *The Journal of Neuroscience*, *33*, 11530–11539.

Felleman, D. J., Lim, H., Xiao, Y., Wang, Y., Eriksson, A., & Parajuli, A. (2015). The representation of orientation in macaque V2: Four stripes not three. *Cerebral Cortex*, *25*, 2354–2369.

Fiorani, M., Azzi, J. C. B., Soares, J. G. M., & Gattass, R. (2014). Automatic mapping of visual cortex receptive fields: A fast and precise algorithm. *Journal of Neuroscience Methods*, *221*, 112–126.

Freeman, J., Ziemba, C. M., Heeger, D. J., Simoncelli, E. P., & Movshon J. A. (2013). A functional and perceptual signature of the second visual area in primates. *Nature Neuroscience*, *16*, 974–981.

Freese, C. H., & Oppenheimer, J. R. (1981). The capuchin monkey, genus *Cebus*. p. 331–389. In A. F. Coimbra-Filho & R. A. Mittermeier (Eds.), *Ecology and behavior of neotropical primates*. Rio de Janeiro, RJ: Academia Brasileira de Ciências.

Friedman, H. S., Zhou, H., & von der Heydt, R. (2003). The coding of uniform colour figures in monkey visual cortex. *Journal of Physiology*, *548*, 593–613.

Gattass, R., Rosa, M. G., Sousa, A. P., Piñon, M. C., Fiorani Júnior, M., & Neuenschwander, S. (1990). Cortical streams of visual information processing in primates. *Brazilian Journal of Medical and Biological Research*, *23*, 375–393.

Gattass, R., Sousa, A. P. B., Mishkin, M., & Ungerleider, L. G. (1997). Cortical projections of area V2 in the macaque. *Cerebral Cortex*, *7*, 110–129.

Gattass, R., Lima, B., Soares, J. G. M., & Ungerleider, L. G. (2015). Controversies about the visual areas located at the anterior border of area V2 in primates. *Visual Neuroscience*, *32*, E019.

Gattass, R., Soares, J. G. M., & Lima, B. (2018). Comparative pulvinar organization across different primate species. *Advances in Anatomy, Embryology and Cell Biology*, *225*, 37–38. doi:10.1007/978-3-319-70046-5_8.

Gegenfurtner, K. R. (2003). Cortical mechanisms of colour vision. *Nature Reviews Neuroscience*, *4*, 563–572.

Gegenfurtner, K. R., Kiper, D. C., & Fenstemaker, S. B. (1996). Processing of color form and motion in macaque area V2. *Visual Neuroscience*, *13*, 161–172.

Hegde, J., & Van Essen D. C. (2000). Selectivity for complex shapes in primate visual area V2. *The Journal of Neuroscience*, *20*, RC60, 1–6.

Hubel, D. H., & Livingstone, M. S. (1985). Complex-unoriented cells in a subregion of primate area 18. *Nature*, *315*, 325–327.

Hubel, D. H., & Wiesel, T. N. (1968). Receptive fields and functional architecture of monkey striate cortex. *Journal of Physiology*, *195*, 215–243.

Johnson, E. N., Hawken, M. J., & Shapley, R. (2008). The orientation selectivity of color-responsive neurons in macaque V1. *The Journal of Neuroscience*, *28*, 8096–8106.

Kiper, D. C., Fenstemaker, S. B., & Gegenfurtner, K. R. (1997). Chromatic properties of neurons in macaque area V2. *Visual Neuroscience*, *14*, 1061–1072.

Kleiner, M., Brainard, D., Pelli, D., Ingling, A., Murray, R., & Broussard, C. (2007). What's new in psychtoolbox-3. *Perception*, *36*, 1–16.

Le Gros Clark, W.E. (1959). *The antecedents of man*. Edinburgh, Scotland: Edinburgh University Press.

Leventhal, A. G., Thompson, K. G., Liu, D., Zhou, Y., & Ault, S. J. (1995). Concomitant sensitivity to orientation, direction, and color of cells in layers 2, 3, and 4 of monkey striate cortex. *The Journal of Neuroscience*, *15*, 1808–1818.

Levitt, J. B., Kiper, D. C., & Movshon, J. A. (1994). Receptive fields and functional architecture of macaque V2. *Journal of Neurophysiology*, *71*, 2517–2542.

Livingstone, M. S., & Hubel, D. H. (1983). Specificity of cortico-cortical connections in monkey visual system. *Nature*, *304*, 531–534.

Livingstone, M. S., & Hubel, D. H. (1984). Anatomy and physiology of a color system in the primate visual cortex. *The Journal of Neuroscience*, *4*, 309–356.

Livingstone, M. S., & Hubel, D. H. (1987). Psychophysical evidence for separate channels for the perception of form color movement and depth. *The Journal of Neuroscience*, *7*, 3416–3468.

Livingstone, M. S., & Hubel, D. H. (1988). Segregation of form color movement and depth: Anatomy physiology and perception. *Acta Crystallographica Section B: Structural Science, Crystal Engineering and Materials*, *240*, 740–749.

Lu, H. D., & Roe, A. W. (2007). Optical imaging of contrast response in macaque monkey V1 and V2. *Cerebral Cortex*, *17*, 2675–2695.

Mazurek, M., Kager, M., & Van Hooser, S. D. (2014). Robust quantification of orientation selectivity and direction selectivity. *Frontiers in Neural Circuits*, *8*, 92. doi:10.3389/ fncir.2014.00092.

Mountcastle, V. B. (1997). The columnar organization of the neocortex. *Brain*, *120*, 701–722.

Munk, M. H., Nowak, L. G., Girard, P., Chounlamountri, N., & Bullier, J. (1995). Visual latencies in cytochrome oxidase bands of macaque area V2. *Proceedings of the National Academy of Sciences of the United States of America*, *92*, 988–992.

Nakamura, H., Gattass, R., Desimone, R., & Ungerleider, L. G. (1993). The modular organization of projections from areas V1 and V2 to areas V4 and TEO in macaques. *The Journal of Neuroscience*, *13*, 3681–3691.

Nascimento-Silva, S., Gattass, R., Fiorani, M. Jr., & Sousa, A. P. B. (2003). Three streams of visual information processing in V2 of Cebus monkey. *Journal of Comparative Neurology*, *466*, 104–118.

Nascimento-Silva, S., Pinõn, C., Soares, J. G. M., & Gattass, R. (2014). Feedforward and feedback connections and their relation to the cytox modules of V2 in Cebus monkeys. *Journal of Comparative Neurology*, *522*, 3091–3105.

Nowak, L. G., Munk, M. H., Girard, P., & Bullier, J. (1995). Visual latencies in areas V1 and V2 of the macaque monkey. *Visual Neuroscience*, *12*, 371–384.

Olavarria, J. F., & Van Essen, D. C. (1997). The global pattern of cytochrome oxidase stripes in visual area V2 of the macaque monkey. *Cerebral Cortex*, *7*, 395–404.

Peterhans, E., & von der Heydt, R. (1993). Functional organization of area V2 in the alert macaque. *European Journal of Neuroscience*, *5*, 509–524.

Roe, A. W., & Tso, D. Y. (1995). Visual topography in primate V2 – Multiple representation across functional stripes. *The Journal of Neuroscience*, *15*, 3689–3715.

Rosa, M. G., Gattass, R., & Fiorani, Jr., M. (1988). Complete pattern of ocular dominance stripes in V1 of a New World monkey, *Cebus apella*. *Experimental Brain Research*, *72*, 645–648.

Shapley, R., & Hawken, M. J. (2011). Color in the cortex: Single- and double-opponent cells. *Vision Research*, *51*, 701–717.

Schiller, P. H., Finlay, B. L., & Volman, S. F. (1976). Quantitative studies of single-cell properties in monkey striate cortex. I. Spatiotemporal organization of receptive fields. *Journal of Neurophysiology*, *39*, 1288–1319.

Shipp, S., & Zeki, S. (1985). Segregation of pathways leading from area V2 to areas V4 and V5 of macaque monkey visual cortex. *Nature*, *315*, 322–324.

Shipp, S., & Zeki, S. (1989). The organization of connections between areas V5 and V2 in macaque monkey visual cortex. *European Journal of Neuroscience*, *1*, 333–354.

Shipp, S., & Zeki, S. (2002). The functional organization of area V2 I: Specialization across stripes and layers. *Visual Neuroscience*, *19*, 187–210.

Silverman, M. S., & Tootell, R. B. H. (1987). Modified technique for cytochrome oxidase histochemistry: Increased staining intensity and compatibility with the 2-deoxyglucose autoradiography. *Journal of Neuroscience Methods*, *19*, 1–10.

Soares, J. G. M., Fiorani, M., Araujo, E. A., Zana, Y., Bonci, D. M. O., Neitz, M., Ventura, D. F., & Gattass, R. (2010). Cone photopigment variations in *Cebus apella* monkeys evidenced by electroretinogram measurements and genetic analysis. *Vision Research*, *50*, 99–106.

Sousa, A. P., Piñón, M. C., Gattass, R., & Rosa, M. G. (1991). Topographic organization of cortical input to striate cortex in the Cebus monkey: A fluorescent tracer study. *Journal of Comparative Neurology*, *308*, 665–682.

Swindale, N. V., Grinvald, A., & Shmuel, A. (2003). The spatial pattern of response magnitude and selectivity for orientation and direction in cat visual cortex. *Cerebral Cortex*, *13*, 225–238.

Tamura, H., Sato, H., Katsuyama, N., Hata, Y., & Tsumoto, T. (1996). Less segregated processing of visual information in V2 than in V1 of the monkey visual cortex. *European Journal of Neuroscience*, *8*, 300–309.

Tootell, R. B., Silverman, M. S., De Valois, R. L., & Jacobs, G. H. (1983). Functional organization of the second cortical visual area in primates. *Science*, *220*, 737–739.

Ungerleider, L. G., & Mishkin, M. (1982). Two cortical visual systems. In D. J. Ingle, M. A. Goodale, & R. J. W. Mansfield (Eds.), *Analysis of visual behavior*. Cambridge, MA: MIT Press.

Ungerleider, L. G., Galkin, T. W., Desimone, R., & Gattass, R. (2014). Subcortical projections of area V2 in the macaque. *Journal of Cognitive Neuroscience*, *26*, 1220–1233.

Webb, A. (2002). *Statistical Pattern Recognition, Second Edition*. Chichester: John Wiley & Sons.

Wong-Riley, M. T., & Carroll, E. W. (1984). Quantitative light and electron microscopic analysis of cytochrome oxidase-rich zones in V II prestriate cortex of the squirrel monkey. *Journal of Comparative Neurology*, *222*, 18–37.

Yoshioka, T., & Dow, B. M. (1996). Color orientation and cytochrome oxidase reactivity in areas V1 V2 and V4 of macaque monkey visual cortex. *Behavioural Brain Research*, *76*, 71–88.

Zeki, S., & Shipp, S. (1988). The functional logic of cortical connections. *Nature*, *335*, 311–317.

Zeki, S., & Shipp, S. (1989). Modular connections between areas V2 and V4 of macaque monkey visual cortex. *European Journal of Neuroscience*, *1*, 494–506.